Nanoindentation of Hard Coatings

Internship report of Niels Consten

Title Page

INFORMATION STUDENT

Name: Niels Consten

Student number: s0182745

INFORMATION UNIVERSITY

Institution: University of Twente

Faculty: Construerende Technische Wetenschappen

Research group: Applied Mechanics

Supervisor: Prof. Dr. Ir. A. de Boer

City and country: Enschede, The Netherlands

INFORMATION INTERNSHIP

Institution: University of Southampton

Faculty: Engineering and the Environment

Research group: national Centre for Advanced Tribology at Southampton (nCATS)

Supervisor: Prof. Dr. Ir. T. Polcar

City and country: Southampton, United Kingdom

Period: March 11, 2013 – May 31, 2013

Preface

This document contains the work done by Niels Consten for his internship as part of the master curriculum of mechanical engineering at the University of Twente. His internship took place at the University of Southampton in the United Kingdom at the research department called *national Centre for Advanced Tribology at Southampton*. During his internship he was supervised by prof. dr. ir. Tomas Polcar and PhD-student ir. Mauro Callisti. His supervisor at his own university was prof. dr. ir. André de Boer. The internship took place from March 11 until May 31 in 2013 containing 5 closure days or bank holidays.

Summary

Nanoindentation measurements were carried out using the coatings CrAlTiN, CrAlSiN (with high Cr/Al ratio), AlCrSiN (with low Cr/Al ratio) and CrAlN deposited by cathodic arc technology on tungsten carbide substrates. For this purposes use is made NanoTest Vantage Platform 4 of Micro Materials with a diamond Berkovich indenter.

The maximum depth of penetration in a test is restricted to no more than 10% of the film thickness to avoid unintentional probing of the properties of the substrate. Hardness and reduced Young's modulus values are extracted from measured load-displacement curves. For statistical purposes, mean values of hardness and reduced Young's modulus are quoted from a set of indentation curves acquired under the same parameters. The data were strongly scattered due to the surface roughness and morphology as the surface exhibits a lot of droplets and holes typical for low-arc cathodic deposition.

The indentation procedure is simulated as a Static Structural Analysis using the Mechanical APDL of ANSYS Workbench 14.0. The indentation procedure is modeled as a 2D axial-symmetric problem. A conical indenter with a semi-angle of $\alpha = 70.3°$ is used as this gives the same area to depth ratio as a triangular Berkovich indenter.

Young's modulus from the nanoindentation measurements serves as input for the model. Linear work hardening is assumed and these plastic material parameters are determined by comparing load-displacement curves from nanoindentation measurements and the finite element simulation.

Tip rounding of the indenter is found to have a big influence on the load-displacement curves and plastic material properties. The radius value of this rounding is not known. Due to this one cannot draw firm conclusions about the found values.

Table of Contents

Table of Symbols

A	Real projected contact area of indenter and coating at full load
A_i	Ideal projected contact area of indenter and coating at full load
a	Contact radius of indenter and coating
β	Dimensionless parameter related to the geometry of the indenter
E	Young's modulus of coating
E_i	Young's modulus of indenter
E_r	Reduced Young's modulus
H	Hardness of coating
h	Displacement of indenter – see below
h_{max}	Displacement of indenter at maximum load – see below
h_p	Penetration depth of indenter into coating at maximum load or plastic depth – see below
h_f	Final penetration depth or residual impression – see below
ν	Poisson's ratio of coating
ν_i	Poisson's ratio of indenter
P	Applied load by indenter on coating
P_{max}	Maximum applied load by indenter on coating
R	Indenter tip radius
T	Tangent modulus of coating for linear work hardening
Y	Yield strength of coating

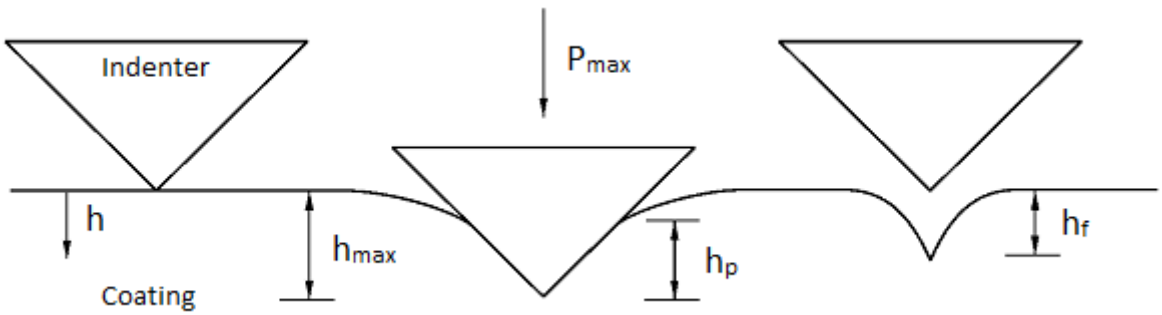

Introduction

The demand for higher cutting speeds and longer service life of cutting tools led to the development and application of hard protective coatings. Titanium nitride (TiN) and chromium nitride (CrN) are widely used in commercial applications and possess good hardness and wear resistant; however, their oxidation resistance is limited to approximately 550 ^{o}C and 700 ^{o}C, respectively. To improve oxidation resistance of these films, ternary systems were investigated, such as Ti-Al-N, Cr-Al-N and Ti-Al-Cr-N, and they are now widely used in commercial applications. Further increase in the oxidation resistance was achieved by the addition of Si or combining nitrides of Ti, Al and Cr in quaternary compounds. The later concept has been found to have promising performance compared to that of ternary films.

The main coating investigated in these report is CrAlTiN, while CrAlSiN (with high Cr/Al ratio), AlCrSiN (with low Cr/Al ratio) and CrAlN are investigated as well. These coatings exhibit excellent oxidation resistant at elevated temperatures (1) (2) (3), but material properties do change at elevated temperatures due to the decrease of dislocation density. Cutting machines operate at very high temperatures, so investigation is required.

This report serves as an initial study. Hardness and Young's modules of these coatings are evaluated at room temperature by depth-sensing indentation or nanoindentation using Platform 4 of NanoTest Vantage from Micro Materials. Unintentional probing of the properties of the substrate is avoided by restricting the maximum depth of penetration in a test to no more than 10% of the film thickness.

A 2D axisymmetric finite element model is made in ANSYS Workbench as well and material properties of the coatings at room temperature are evaluated. To this purposes, linear work hardening behavior is assumed. The Young's modulus and maximum indentation depth from the experiments serves as input variables. Yield strength and tangent modulus are found by comparing load-displacement curves of both experiments and simulation.

Future studies can use this model to evaluate material properties of the coatings at elevated temperatures.

Work Plan

Depth-sensing Indentation

The goal of the majority of depth-sensing indentation or nanoindentation tests is to extract hardness and Young's modulus of the specimen material from load-displacement measurements. Conventional indentation hardness tests involve the measurement of the size of a residual plastic impression in the specimen as a function of the indenter load. This provides a measure of the area of contact for a given indenter load. In a nanoindentation test, the size of the residual impression is often only a few microns and this makes it very difficult to obtain a direct measure using optical techniques. In nanoindentation testing, the depth of penetration beneath the specimen surface is measured as the load is applied to the indenter. The known geometry of the indenter then allows the size of the area of contact to be determined. The procedure also allows for the modulus of the specimen material to be obtained from a measurement of the 'stiffness' of the contact, that is, the rate of change of load and depth.

The chief difficulty encountered in nanoindentation of coatings/thin films is to avoid unintentional probing of the properties of the substrate. To avoid this, it is common to restrict the maximum depth of penetration in a test to no more than 10% of the film thickness, although research suggests that this rule has no physical basis. Furthermore, it is concluded that Young's modulus of thin films responds more sensitively to the mechanical properties of the substrates than does the hardness.

For this purposes use is made of NanoTest Vantage Platform 4 of Micro Materials with a diamond Berkovich indenter.

Experimental Settings

Hardness and Young's Modulus measurements were carried out using the coatings CrAlTiN, CrAlSiN (with high Cr/Al ratio), AlCrSiN (with low Cr/Al ratio) and CrAlN deposited by cathodic arc technology on tungsten carbide substrates. Some details are listed in table 1. (1) (2)

Coating	Cr (at.%)	Al (at.%)	Ti (at.%)	Si (at.%)	N (at.%)	O (at.%)	Thickness
CrAlTiN	16	31	7	0	46	0	2.4
CrAlSiN	29.9	25.6	0	3.8	39.1	1.7	2.1
AlCrSiN	17.4	32.7	0	3.3	44.3	2.3	2.3
CrAlN	25.0	31.0	0	0.1	40.0	3.8	2.2

Table 1 - Properties coatings

Nanoindentation measurements of these coatings are performed under constant load rate control (2 mN/s). When the final specified depth is reached, a constant load is maintained for 20 seconds to allow for possible creep before the unloading with a constant load rate control (1 mN/s) is performed. Thermal drift is accounted for as well by maintaining a constant load for 30 seconds during unloading at 10% of maximum load. A load-displacement curve for CrAlTiN is shown in figure 1. Note that the maintained constant loads are clearly visible in the graph.

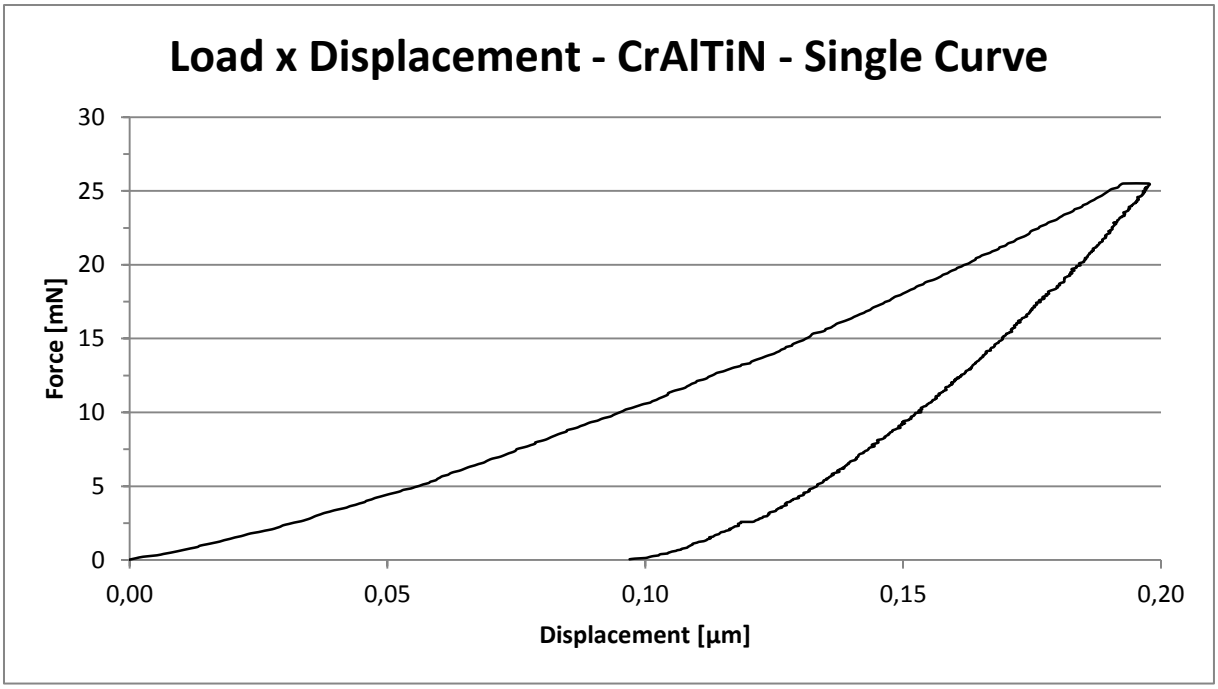

Figure 1 - Single load-displacement cuve CrAlTiN at 200nm

For statistical purposes, it is good practice to quote mean values of hardness and reduced Young's modulus from a set of indentation curves acquired under the same parameters.

For CrAlTiN indentations were performed at 100, 150, 200, 250 and 500 nm as well as at a load of 500 mN (approximately 1100 nm). At each depth 40 indentations were carried out at two different spots of the sample, except at 200 nm and 500 mN. At these depths 60 at three different spots and 20 indentations at one spot respectively were performed. The offset between each indentation was 50 µm to avoid influences of neighbor indentations.

For CrAlSiN, AlCrSiN and CrAlN only 40 indentations at two different spots of the samples were performed with a specified depth of 200 nm. This is approximately the mentioned 10% thickness of the coatings. Surface effects on one hand and substrate effects on the other hand are minimized at that depth.

Analysis

As reported by Oliver and Pharr (4) and Brotzen (5) the effects of a non-rigid indenter on the load-displacement behavior can be taken into account by defining a reduced Young's modulus. This modulus is related to the indenter and specimen (coating in this report) by

$$\frac{1}{E_r} = \frac{1-\nu^2}{E} + \frac{1-\nu_i^2}{E_i}, \qquad (1)$$

where E is Young's modulus and ν is the Poisson's ratio of the specimen, and E_i and ν_i are the same parameters for the indenter. E_r is evaluated from the nanoindentation measurements according to the following equation

$$E_r = \frac{1}{2\beta}\sqrt{\frac{\pi}{A}}\left(\frac{dP}{dh}\right)_{unload}, \qquad (2)$$

where P is the indenter load, h the penetration depth and $(dP/dh)_{unload}$ is the slope of the unloading curve evaluated at the position of maximum load, see figure 2. A is the projected contact area at full load and β is a dimensionless parameter related to the geometry of the indenter. In the case of a Berkovich indenter one finds $\beta = 1.034$.

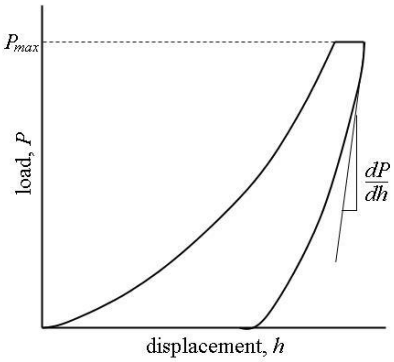

Figure 2 – Load-displacement curve

For evaluating the reduced Young's Modulus, the slope $(dP/dh)_{unload}$ and the projected contact area A should be determined precisely. A least mean square fit to 60% of the unloading curve is made according to the prediction by the Hertz equations that the unloading data will be better expressed by a power law

$$P = a(h - h_f)^m, \tag{3}$$

where a and m are the parameters to be fitted and h_f is the final penetration depth or residual impression, see figure 3. The equation is then analytically differentiated for determining the slope $(dP/dh)_{unload}$.

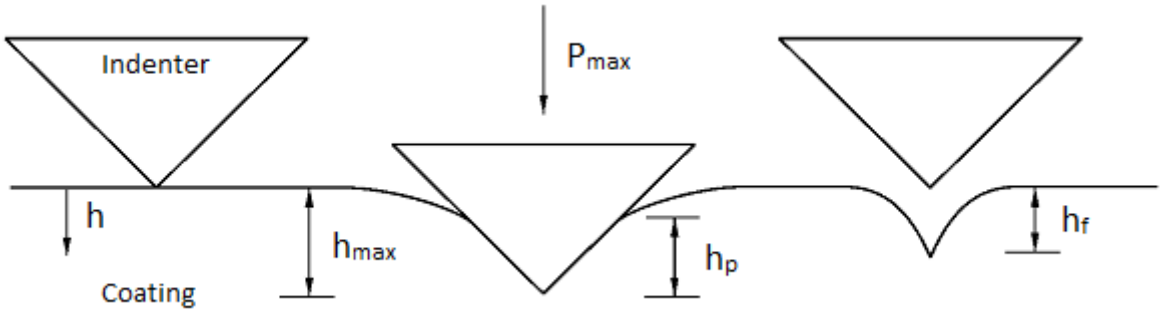

Figure 3 - Depth definitions

The penetration depth at maximum load or plastic depth h_p for a Berkovich indenter is found from

$$h_p = h_{max} - 0.75 P_{max} \left(\frac{dh}{dP}\right)_{unload}, \tag{4}$$

where h_{max} is the depth at maximum load and P_{max} is the maximum load, see figure 3.

The projected contact area of the indenter at maximum load can be found from geometry. However, to account for non-ideal geometry of the indenter like rounding of the indenter tip and other defects, it is nowadays regular practice to use an indirect method for determining projected area functions. The procedure is to perform a series of indentations at varying maximum load or displacement on standard test specimens whose elastic modulus and Poisson's ratio are known. In this study isotropic fused Silica is used. If E_r is known (embodying the elastic properties of both indenter and specimen with equation 1), then the actual projected area of contact at each load is found from equation 2. Values of A and h for each test on the reference material provide the data for a projected area function of the form

$$A(h_p) = C_1 h_p^2 + C_2 h_p. \quad (5)$$

Reduced Young's modulus of the coating is now obtained from equation 2, and the hardness H is given by the well-known relation

$$H = \frac{P_{max}}{A}. \quad (6)$$

Almost all of these analyzes is done by the computer software NanoTest Vantage Platform 4 by Micro Materials (6). The output data of the software is the hardness and the reduced Young's Modulus for each single indentation, corrected for creep and thermal drift. Instrument compliance is taken into account as well by the software, as the measured unloading stiffness has contribution from both the responses of the specimen and the instrument. The contribution from the instrument includes the compliance of the loading frame, the indenter shaft, and the specimen mount.

Finite Element Model

In the present work, the indentation procedure is simulated as a Static Structural Analysis using the Mechanical APDL of ANSYS Workbench 14.0. It is assumed that the material behaves isotropic and homogeneous. The coating and indenter are treated as isothermal and body forces are neglected. Creep and thermal drift is excluded as well, as there is no time dependency taken into account. Furthermore, the coating is assumed to be initially stress free and in perfect contact during indentation process.

Material properties

Lichinchi et al. simulated load-displacement curves of indentation on TiN-coatings for rigid and deformable indenters and showed good agreement between both finite element models (7). In the present study, it is chosen to model the indenter as a rigid indenter in order to reduce simulation time and to overcome convergence issues. It is not possible to set the body behavior to *rigid* in axial-symmetric 2D analyses (8), so a large value has to be assigned to the Young's modulus of the indenter with respect to the coating. S. Sezer (9) observed that there was no difference in results when the ratio between Young's moduli of indenter and coating was 10^6 or 10^7, so this ratio is set to 10^6 for all simulations. No plasticity is taken into account for the indenter.

For the coating, both elasticity and plasticity have to be accounted for. Linear elasticity is assumed and Young's modulus of depth-sensing indentation measurements is used as input parameter. According to plasticity, for most materials strain-hardening occurs due to the pile-up and interaction between dislocations in the material. These interactions serve to make the material harder. To account for this behavior, linear work hardening obeying the von Mises yield criterion is assumed.

Geometry

The indentation procedure is modeled as a 2D axial-symmetric problem, see figure 4. To this purposes a conical indenter with a semi-angle of $\alpha = 70.3°$ is used as this gives the same area to depth ratio as a triangular Berkovich indenter. Lichinchi et al. also simulated loading-unloading curves of indentations on TiN-coatings with a three-dimensional Berkovich model and a 2D axial-symmetric conical model with the same semi-angle. The curves were practically identical indicating that the axial-symmetric model is an effective tool for simulating nanoindentation procedure with a Berkovich indenter (7). The indenter is modeled with a rounding tip and is evaluated for two different radii. As the thickness of the coating is around 2.4 µm, the coating is modeled as 2.4 µm by 2.4 µm, see figure X. Doubling the coating width has a small influence on load-displacement curves as shown in Appendix 'Width' The substrate is not modeled as penetration does not exceed 10% of the thickness of the coating.

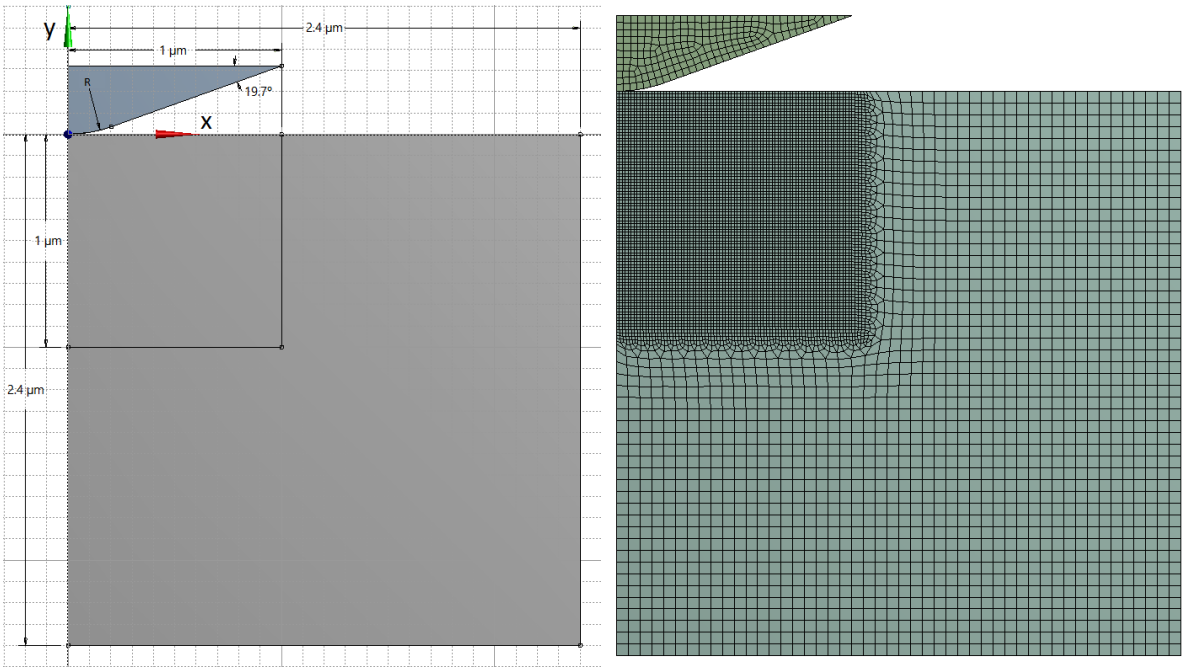

Figure 4 - Dimensions and mesh indentation simulation

Contact Region

All contact problems require a stiffness between the two contact surfaces. The amount of penetration between the two surfaces depends on this stiffness. Higher stiffness values decrease the amount of penetration but can lead to ill-conditioning of the global stiffness matrix and to convergence difficulties. Ideally, you want a high enough stiffness that contact penetration is acceptably small, but a low enough stiffness that the problem will be well-behaved in terms of convergence or matrix ill-conditioning (10).

For surface-to-surface contact elements, ANSYS uses either the augmented Lagrangian method (default) or the penalty method. The augmented Lagrangian method is an iterative series of penalty updates to find the exact Lagrange multipliers (i.e. contact tractions). Compared to the penalty method, the augmented Lagrangian method usually leads to better conditioning and is less sensitive to the magnitude of the contact stiffness coefficient. However, in some analyses, the augmented Lagrangian method may require additional iterations, especially if the deformed mesh becomes too distorted (10).

If one surface is stiffer than the other, the softer surface should be the contact surface and the stiffer surface should be the target surface (10).

It is for that reason that target elements are assigned to the indenter edge and contact elements the thin film edge. Furthermore, in this study the augmented Lagrangian is used to avoid ill-conditioning. Gauss Integration Points detection mode was selected and the contact stiffness is updated at each iteration to minimize convergence issues. Friction between contacting edges is neglected as for indenters with large semi-angles frictional effects are very small (11).

Mesh

Use is made of planar Q8 elements (PLANE183) for both coating and indenter. In total 9453 elements are used. As already mentioned, target elements (TARGE169) are assigned to the contact edge of the

indenter and contact elements (CONTA172) to the contact edge of the coating. The mesh is refined around the indentation region, see figure 4. To this purposes, a Boolean operator was used on the coating body.

Boundary conditions

The nodes along the axis of rotation (y-axis) for the indenter and the coating are constrained in x-direction, so

$$u(0, y) = 0. \tag{7}$$

The nodes along the bottom edge of the coating are constrained in x-direction and y-direction, so

$$v(x, -2.4) = 0. \tag{8}$$

$$u(x, -2.4) = 0, \tag{9}$$

One could choose not to constrain the nodes along the bottom edge in the x-direction, although it is shown in Appendix 'Boundary Conditions' that is has only a small influence on the load-displacement curves.

The nodes along the top edge of the indenter are subjected to a displacement in y-direction. This contains two steps: loading, where the maximum depth is prescribed, and unloading, where its initial position is prescribed again.

Furthermore, the indenter and coating are initially in contact to avoid rigid body motion, which is not allowed in static structural analysis.

Analysis Settings

The problem contains a few non-linearity's:

- Material properties are non-linear due to the plasticity model.
- Contact between bodies is a non-linear problem.
- Large deformations under the indenter exclude linear theory.

To solve this non-linear problem, the Newton-Raphson method is used. To overcome convergence issues, enough substeps are required for both steps: loading and unloading. Approximately 360 substeps are required to simulate the indentation. For the same reason, displacement is prescribed instead of force at the top edge of the indenter.

Solution

The reaction force in y-direction at the bottom edge of the coating is measured and plotted against the prescribed displacement of the indenter to obtain load-displacement curves.

Validation

In order to verify whether the model behaves properly, load-displacement curves are compared with load-displacement curves found in literature (7). Lichinchi et al. compared their finite element models with experimental data on TiN coatings, see figure 5, and they used material data displayed in table 2 assuming linear elastic rigid plastic material behaviour. The load-displacement curve of the model used in this study with the same material data for the rigid indenter simulation is shown in

figure 5. A good agreement between both figures is observed, so the model in this study is believed to behave properly.

	Material	E [GPa]	v [-]	Y [GPa]	H [GPa]
Flexible Indenter	TiN	418	0.25	14.5	27
	Diamond	1141	0.07	35.7	98
Rigid Indenter	TiN	301	0.25	14.5	27
	Diamond	-	-	-	-

Table 2- Material properties TiN coating for rigid plasticity model by Lichinchi et al

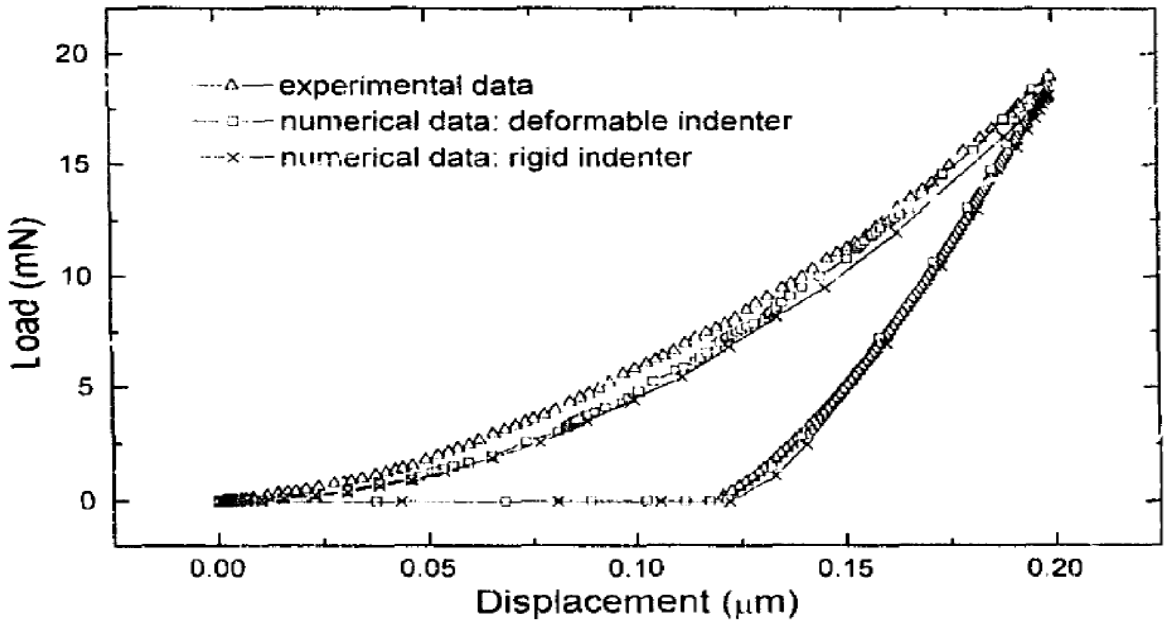

Figure 5 Load-displacement curves TiN coating for rigid plasticity model by Lichinchi et al.

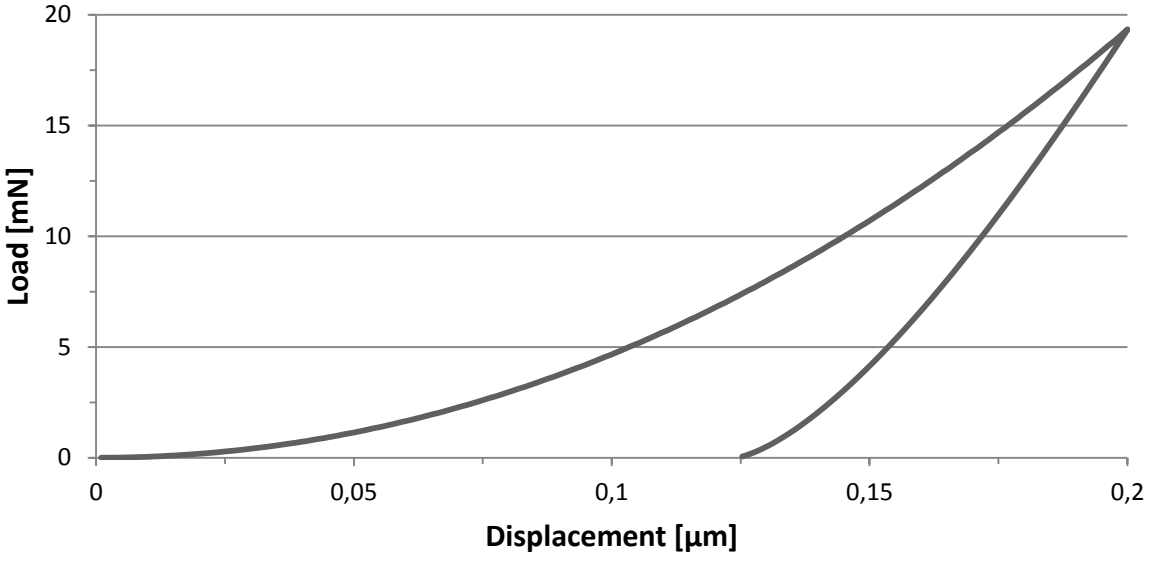

Figure 6 - Load-displacement curve TiN coating for rigid plasticity model for rigid indenter in this study

Modeling

The next step is to use the finite element model to simulate the depth-sensing indentation measurements. Measurements at a specified depth of 200 nm (approximately 10% of the coating thickness) are considered, as unintentional probing of the properties of the surface and the substrate have to be avoided. To this purposes, some representative load-displacement curves from the nanoindentation measurements are compared with load-displacement curves from simulation. 'Representative' in this particular case means curves with hardness, Young's modulus, depth at maximum load and residual depth values closest to the average values of all selected measurements. Dwelling periods to account for creep and thermal drift are removed from the load-displacement curves from the measurements.

For the elastic part of the finite element model, the Young's modulus determined from measurements is used. One should notice that not the real or reduced Young's modulus from measurements is taken into account, as calculated by equation 1, but the Young's modulus calculated by the following equation is used:

$$\frac{1}{E_r} = \frac{1-\nu^2}{E}. \qquad (10)$$

The most right term in equation 1 becomes zero due to the very large Young's modulus of the rigid indenter in the model appearing in the denominator of the second term on the right side.

Furthermore the average Poisson ratio of CrN, AlN and TiN, see table 3, and the average depth at maximum load of all selected indentations is used as input variables for the model.

Material	CrN	AlN	TiN	CrAlTiN
ν [-]	0.29	0.22	0.25	0.25

Table 3 - Poisson's ratio for different coatings

Two different radii are considered: **R=250** nm for all coatings and **R=600 nm** for CrAlTiN only. The first one is believed to be the real tip rounding of the Berkovich indenter used for nanoindentation measurements. As it was not completely certain and it was not possible to perform a SEM (Scanning Electron Microscope) analysis, a calculations was performed for which it was found that the radius for CrAlTiN could be R=600. The calculation is found in the next section.

The two parameters for the plastic material properties remain, namely the yield strength Y and tangent modulus T as linear work hardening is assumed. These values are found iteratively doing a lot of simulations for different values and comparing the load-displacement curves of simulation and experiments: Residual depth and maximum load of these simulations are compared with the average residual depth and average maximum load from measurements. Therefore, in theory there should be one solution for the plastic material properties.

Results

CrAlTiN

Hardness & Young's modulus

The results of the depth-sensing indentation on CrAlTiN at 27°C are displayed in figure 8 and 9 and table 4. The data were strongly scattered due to the surface roughness and morphology as the surface exhibits a lot of droplets and holes typical for low-arc cathodic deposition, see figure 7. Even curve selection about half the total amount of indentations did not yield a hardness value with standard deviation lower than 5 GPa and a reduced Young's Modulus value with standard deviation lower than 34 GPa at most depths. This is even worse at shallow depths. Substrate effects are clearly observable at 500 mN depth (approximately 1100 nm). From that perspective it may be concluded that the values for hardness and reduced Young's Modulus between 200 nm and 500 nm are most representative for the coating, as surface effects on one hand and substrate effects on the other hand are minimized. It is also observed that Young's modulus responds more sensitively to the mechanical properties of the substrates than does the hardness.

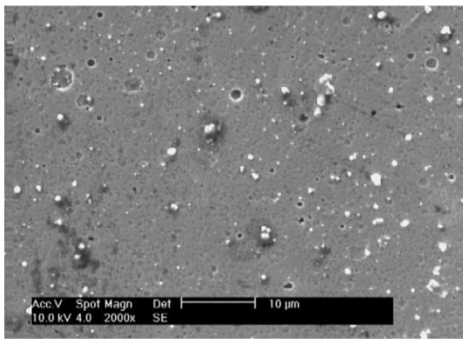

Figure 7 - SEM micrograph of CrAlTiN

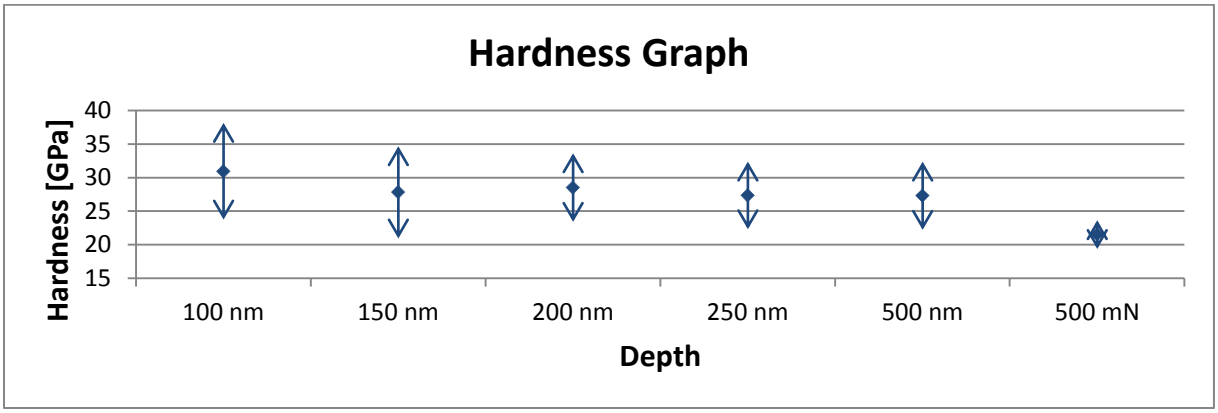

Figure 8 - Hardness of CrAlTiN at different depths

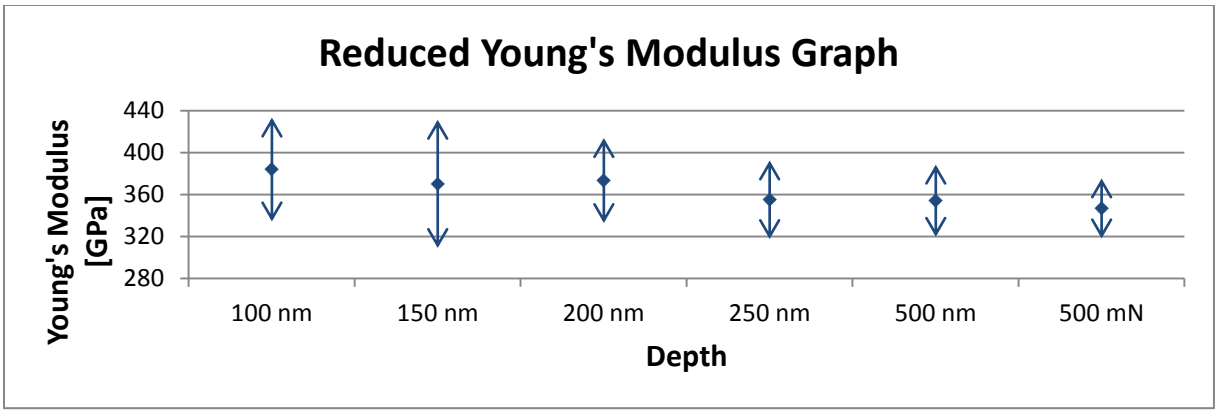

Figure 9 - Reduced Young's modulus of CrAlTiN at different depths

Depth	Hardness [GPa]		Reduced Young's Modulus [GPa]	
	Average	Standard Deviation	Average	Standard Deviation
100 nm	30.9	7.2	383.9	49.6
150 nm	27.8	6.9	370.0	61.1
200 nm	28.5	5.1	373.3	40.5
250 nm	27.3	5.0	355.1	37.5
500 nm	27.3	5.1	354.0	34.3
500 mN	21.5	2.1	346.7	28.5

Table 4- Hardness and reduced Young's modulus of CrAlTiN at different depths

Although it is convenient to express the elastic material properties in terms of reduced Young's modulus as Poisson's ratio is often not known, it is possible to express it in terms of the real Young's modulus by assuming Poisson's ratio. Considering the material properties of the diamond Berkovich indenter, see table 2 and equation 1, one finds the real Young's moduli at different depths, see table 5. Poisson's ratio of the coating is assumed to be the averaged of CrN, AlN and TiN, see table 3.

Depth	100 mN	150 mN	200 mN	250 mN	500 mN	500 mN
Young's Modulus [GPa]	541.1	512.2	518.9	482.2	480.1	465.9

Table 5 - Young's modulus CrAlTiN at different depths

Model

The yield strength and tangent modulus for CrAlTiN assuming linear work hardening are evaluated to be $Y = 10.5\,GPa$ and $T = 99\,GPa$ respectively for a tip rounding of $R = 250nm$. The load-displacements curves of simulation and a few measurements are shown in the figure below.

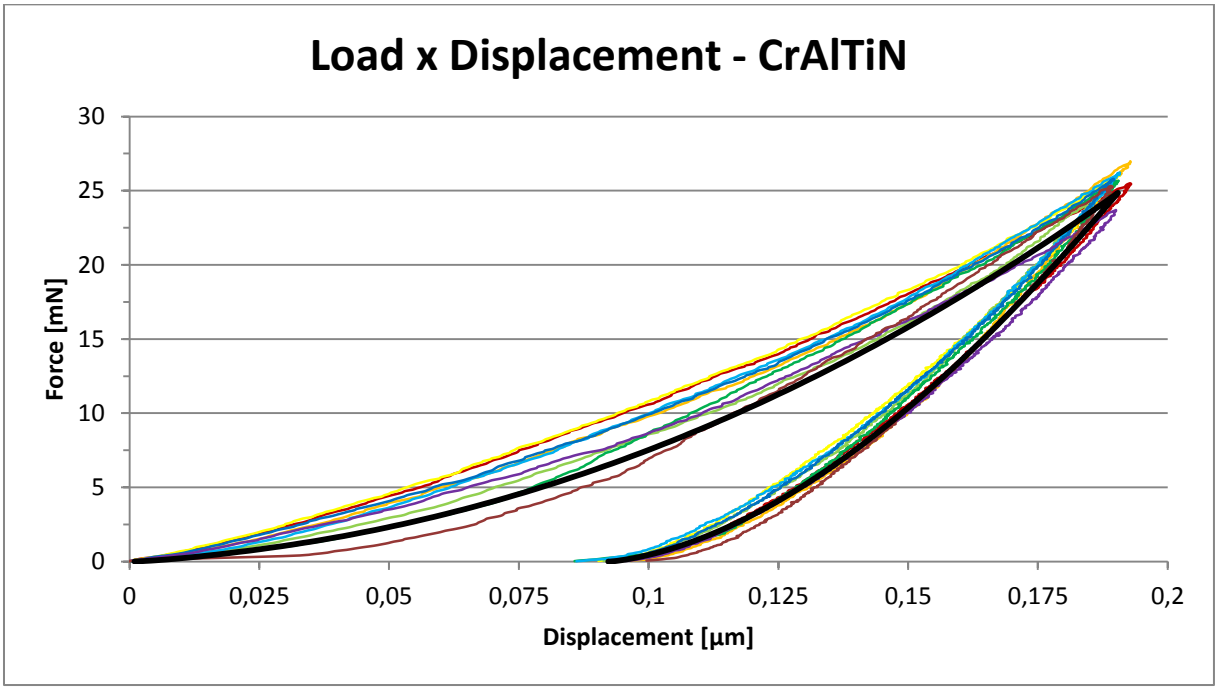

Figure 10 - Load-displacement curves of simulation (black) and measurements (colors) for CrAlTiN with R=250nm

CrAlN, CrAlSiN & AlCrSiN

Hardness & Young's modulus

The results of the depth-sensing indentation on CrAlN, CrAlSiN and AlCrSiN at 26°C are displayed in figure 11 and 12 and table 6. Nanoindentation was performed at a depth of 200 nm as the coating thickness for CrAlN, CrAlSiN and AlCrSiN was 2.2, 2.1 and 2.3 µm respectively. The data were again strongly scattered due to the surface roughness and morphology and curve selection about half the total amount of indentations did not yield hardness and reduced Young's modulus values with small deviation. Even no single curve of AlCrSiN was appropriate for analysis.

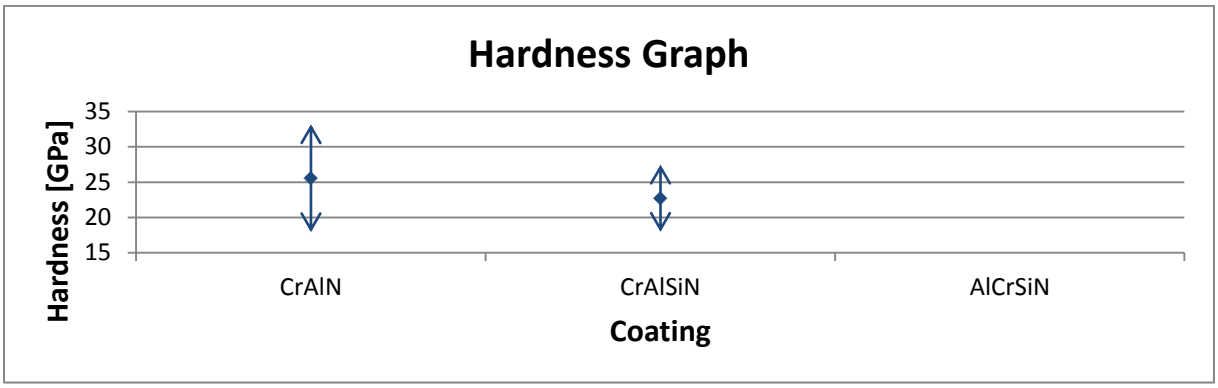

Figure 11 - Hardness of CrAlN, CrAlSiN and AlCrSiN

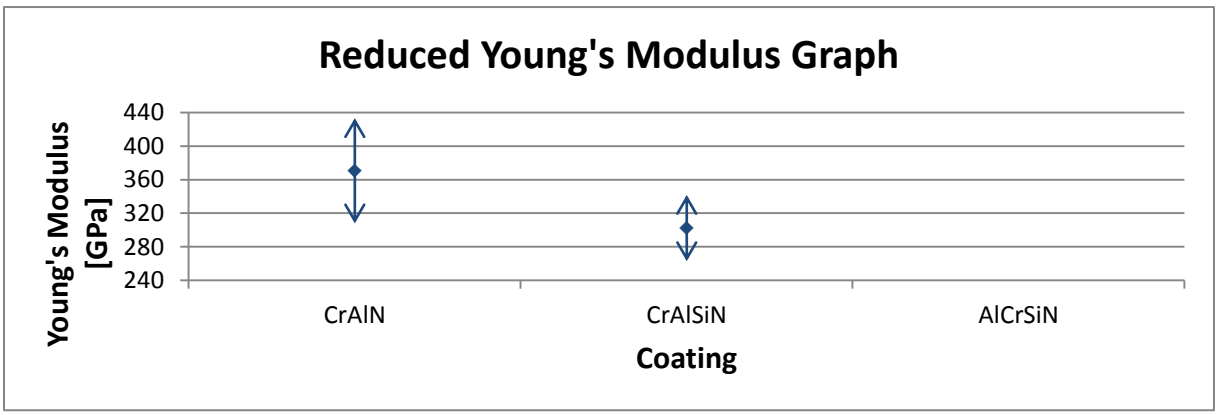

Figure 12 - Reduced Young's modulus of CrAlN, CrAlSiN and AlCrSiN

Coating	Hardness [GPa]		Reduced Young's Modulus [GPa]	
	Average	Standard Deviation	Average	Standard Deviation
CrAlN	25.6	7.7	370.7	62.8
CrAlSiN	22.7	4.8	302.3	39.5
AlCrSiN	-	-	-	-

Table 6 - Hardness & reduced Young's modulus of CrAlN, CrAlSiN and AlCrSiN

Model

The yield strength and tangent modulus for CrAlSiN assuming linear work hardening are evaluated to be $Y = 500\ MPa$ and $T = 141.5\ GPa$ respectively. The load-displacements curves of simulation and a few measurements are shown in the figure below.

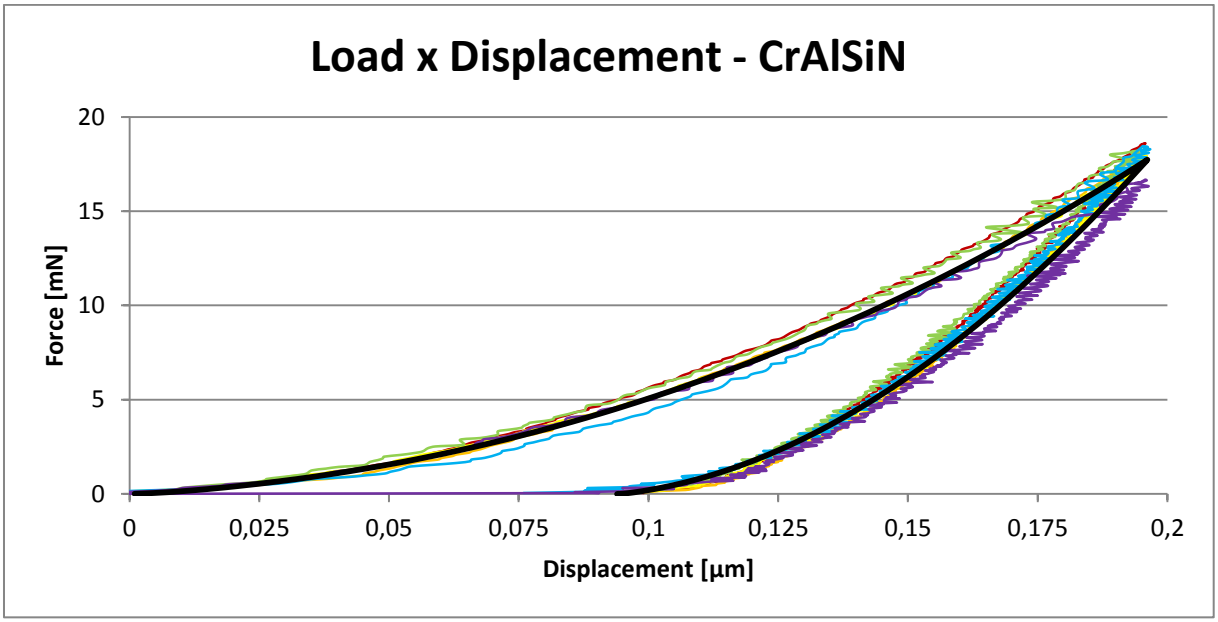

Figure 13 - Load-displacement curves of simulation (black) and measurements (colors) for CrAlSiN with R=250nm

The yield strength and tangent modulus for CrAlTiN assuming linear work hardening are evaluated to be $Y = 200\ MPa$ and $T = 170\ GPa$ respectively. The load-displacements curves of simulation and a two measurements are shown in the figure below.

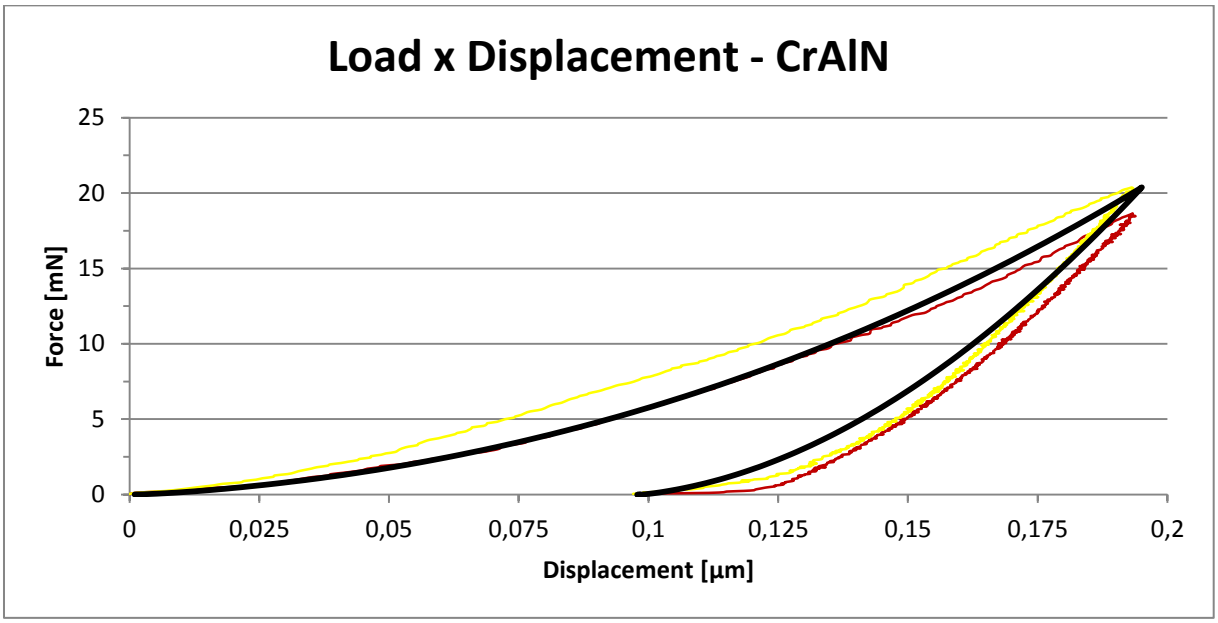

Figure 14 - Load-displacement curves of simulation (black) and measurements (colors) for CrAlN with R=250nm

Indenter Geometry

As mentioned before, the area of contact at penetration depth h_p can be found from geometry. This assumes that the geometry of the indenter is ideal, a circumstance impossible to achieve in practice. To account for non-ideal geometry of the indenter used in any practical test, it is necessary to apply a correction factor to this equation, so as to determine the real area of contact at penetration depth h_p. To this purposes a projected area function was determined. To obtain some information about the indenter, the area correction function is shown in figure 15. The ideal projected area A_i and the real projected area A are calculated by

$$A_i = 24.5h_p^2, \tag{11}$$

$$A = \frac{P_{max}}{H}, \tag{12}$$

where the plastic depth h_p, maximum load P_{max} and hardness H are the values of the nanoindentation measurements at each depth.

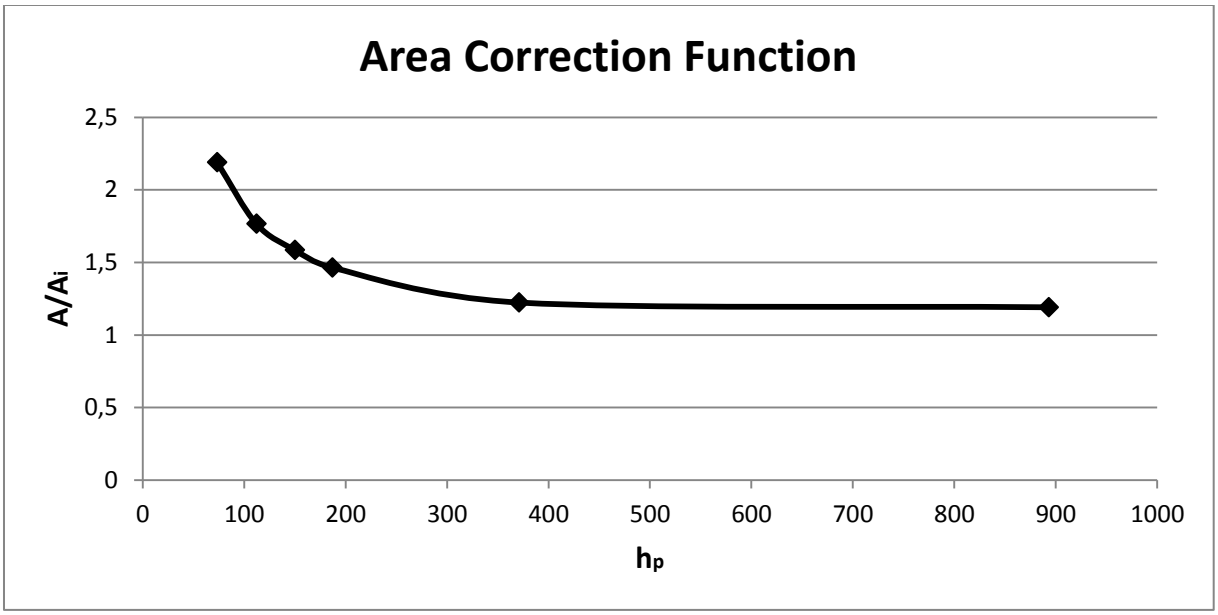

Figure 15 - Area correction function for indentation of CrAlTiN

Tip Rounding

The large value of A/A_i at low depths is a consequence of the inevitable bluntness of the indenter tip. In fact, Berkovich indenters are not perfectly sharp but have a tip radius in the order of 100nm. Figure 16 shows a few finite element simulations for different radii of the tip. It is clearly visible that the rounding tip has a big influence on the load-displacement curve. As a consequence, this should be taken into account for the finite element model.

But can we say something about the tip rounding radius? As the real projected area A and penetration depth h_p at each indentation depth is known by measurements, one can calculate what the radius in the finite element model should be. According to figure 17 one finds from geometry that:

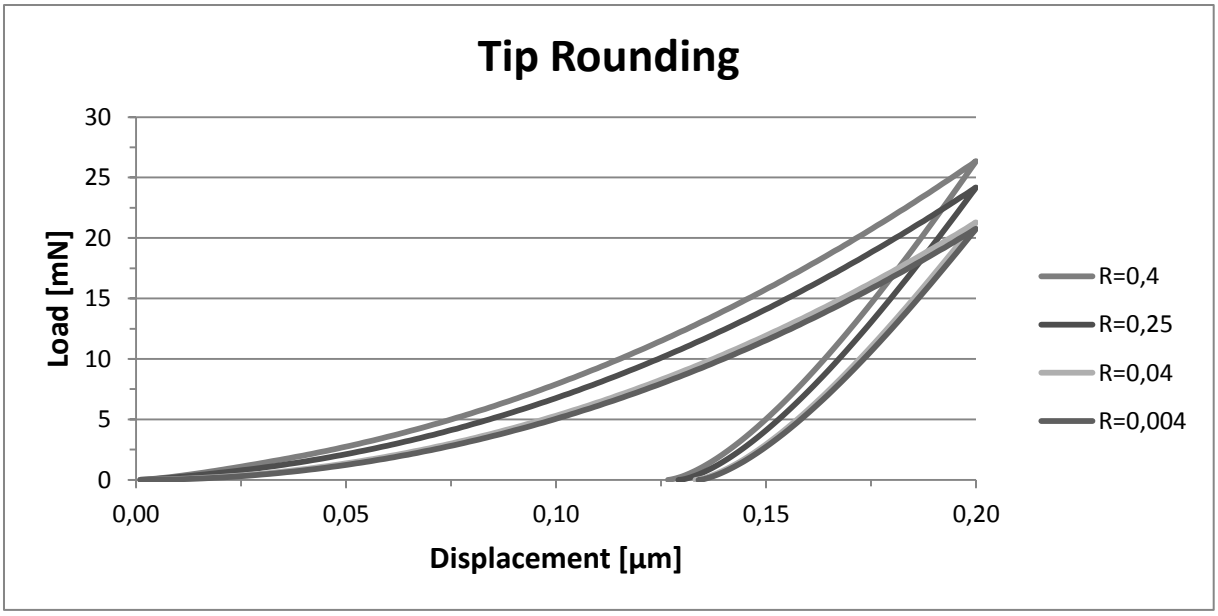

Figure 16 - Influence of tip rounding on simulations

$$h_p = R(1 - \sin 70.3°) + \frac{a - \mathrm{R}\cos 70.3°}{\tan 70.3°},$$

$$h_p \tan 70.3° = R \tan 70.3° (1 - \sin 70.3°) - \mathrm{R}\cos 70.3° + a, \qquad (13)$$

$$R = \frac{h_p \tan 70.3° - a}{\tan 70.3° (1 - \sin 70.3°) - \cos 70.3°},$$

where R is the radius of the tip and a the contact radius of indenter and coating. The contact radius is calculated from

$$a = \sqrt{\frac{A}{\pi}} \qquad with \qquad A = \frac{P}{H} \qquad (14)$$

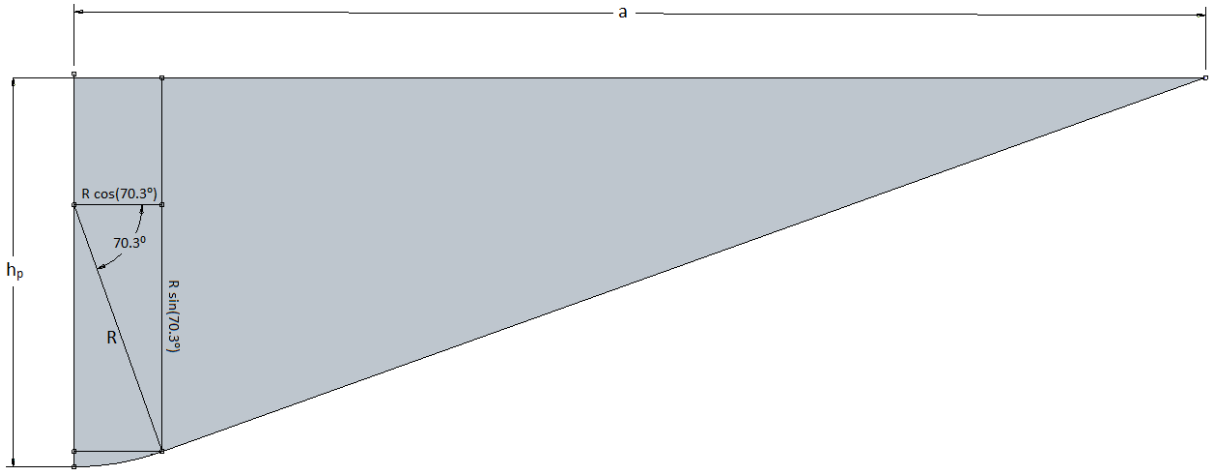

Figure 17 - Indenter geometry with tip for simulation

The outcome of the calculation for CrAlTiN is shown in table 7. It is clear that rounding of the tip is indeed in the order of 100nm, although an exact value cannot be given. The calculation does only

consider a perfectly rounding tip rather than a blunt tip. Probably, the penetration depth for both experiment and simulation will also differ due to numerical limitations. Furthermore the penetration depth from the nanoindentation measurements is calculated and not measured as that is impossible. This calculation may also be uncertain as pile up or sink in behavior is not considered in this calculation.

Depth	Radius [nm]
100 nm	565.6
150 nm	431.5
200 nm	624.4
250 nm	631.4
500 nm	632.2
500 mN	1309.0

Table 7 - Calculated radius of indenter for CrAlTiN indentation

The outcome for CrAlN and CrAlSiN is shown in table 8. A tip radius of approximately 1300 nm is found. As the calculation is a bit arbitrary, only $R = 600\ nm$ for CrAlTiN is considered.

Coating [200 nm]	Radius [nm]
CrAlN	1321
CrAlSiN	1355

Table 8 - Calculated radius of indenter for CrAlSiN and CrAlN indentation

Model

The yield strength and tangent modulus for CrAlTiN assuming linear work hardening are evaluated to be $Y = 470\ MPa$ and $T = 174\ GPa$ respectively for a tip rounding of $R = 600\ nm$. The load-displacements curves of simulation and a few measurements are shown in the figure below.

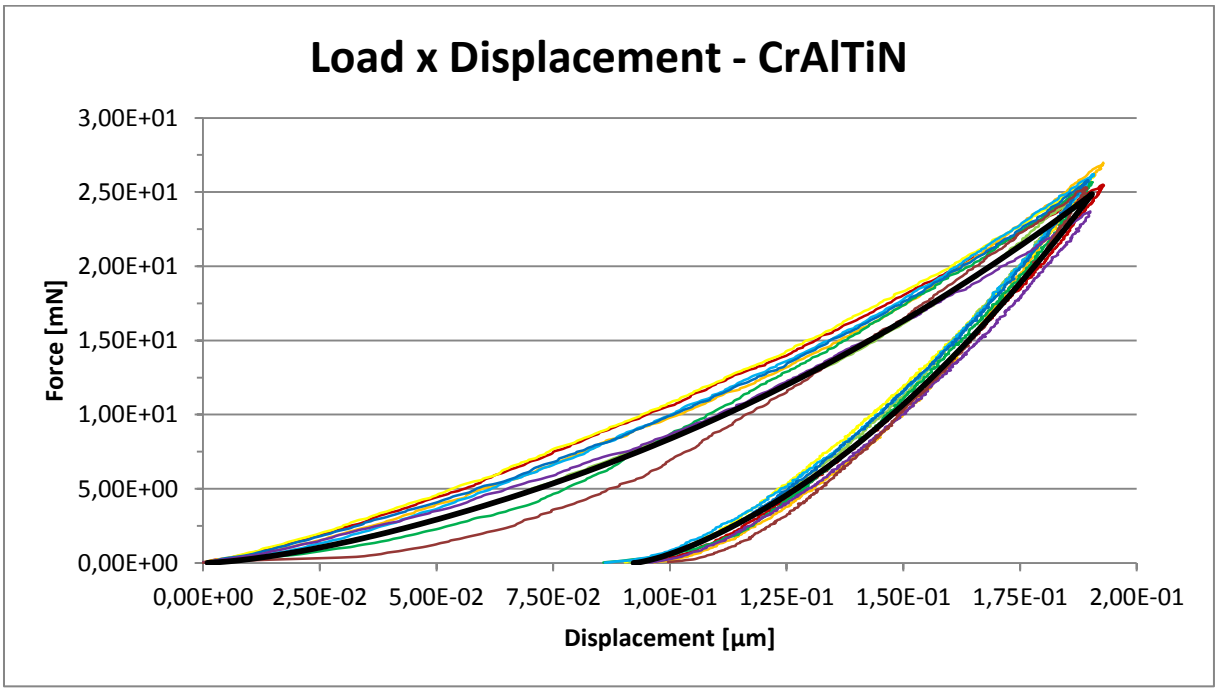

Figure 18 - Load-displacement curves of simulation (black) and measurements (colors) for CrAlTiN with R=600nm

The load-displacements curves of simulations of CrAlTiN for $R = 250\,nm$ and $R = 600\,nm$ are compared and shown in the figure below. It is clear that the loading part is beter described by the simulation for $R = 600\,nm$ and that the unloading part by the simulation for $R = 250\,nm$.

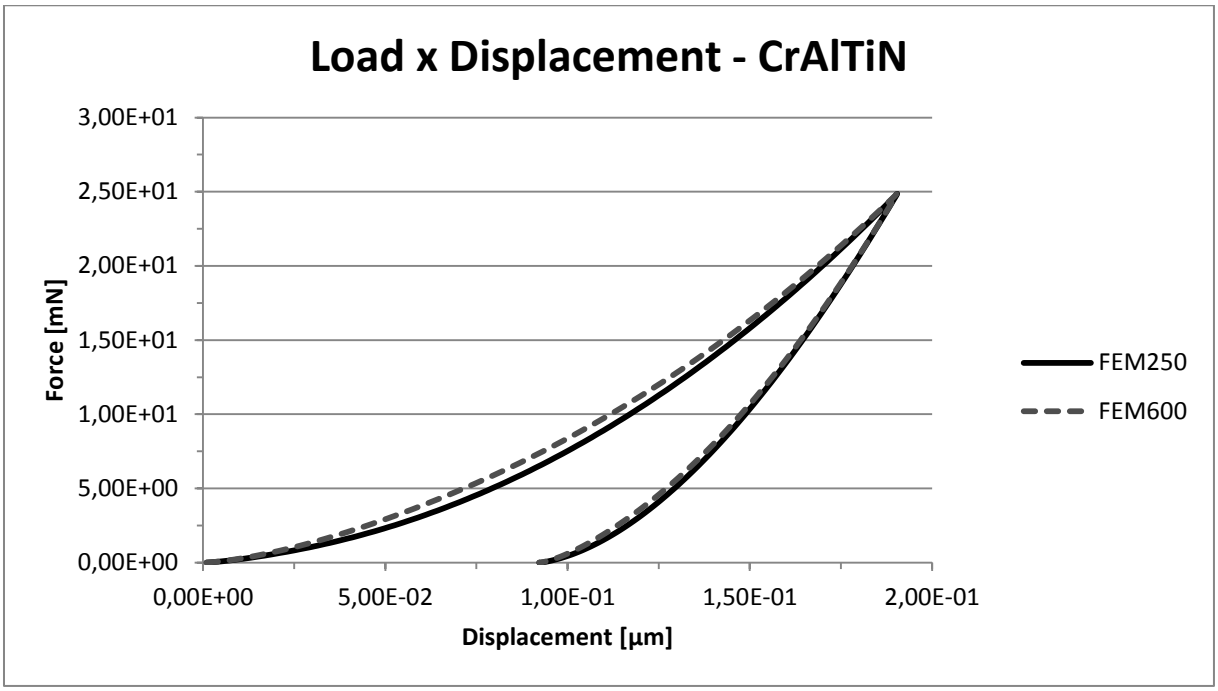

Figure 19 - Load-displacement curves of simulation with different radii for CrAlTiN

Conclusions

The results of the nanoindentation measurements and finite element simulations are summarized in table 20.

Coating	R [nm]	H [GPa]	E [Gpa]	Y [GPa]	T [GPa]
CrAlTiN	250	28.5	520	10.5	99
	600	28.5	520	0.47	174
CrAlN	250	25.6	515	0.20	170
CrAlSiN	250	22.7	385	0.50	141.5
AlCrSiN	--	-	-	-	-

Figure 20 - Material properties coatings found by measurements and simulation

Previous studies found hardness values of 38, 30, 27 and 36 GPa for CrAlTiN, CrAlN, CrAlSiN and AlCrSiN respectively. (1) (2) These values were believed to be way too high, so in that perspective the values found in this report could be right. However, it is still not possible to conclude that these values are right as the data were strongly scattered due to the surface roughness and morphology. Even curve selection about half the total amount of indentations did not yield a hardness values with low standard deviations.

On the other hand results at different depths for CrAlTiN did follow an expected trend: Hardness and Young's modulus values decrease with increasing penetration depth as substrate effects become more sensible.

Plastic material properties found by simulation are uncertain as well. The biggest concern is the radius of the tip rounding. Simulations on CrAlTiN show very big influences of tip rounding on the plastic material properties.

Another concern is the linear work hardening assumption. The assumption seems to be justified for CrAlSiN looking at the load-displacement curves, see figure 13, although some nanoindentation measurement curves contain a certain vibration. It is not known what the source is of this vibration. The linear work hardening seems to be more justifiable for CrAlTiN with a tip radius of 600 nm than 250 nm, see figure 19. Not enough representative curves of CrAlN are available to draw conclusions for that coating about the plasticity model.

Yield strengths for most hard coatings are in the order of 100 MPa, so in that perspective the plastic material properties for CrAlTiN with a radius of 250 nm seem unrealistic. The others do have yield strengths of that order.

Recommendations

As mentioned before, the data of the experiments were strongly scattered due to the surface roughness and morphology as the surface exhibits a lot of droplets and holes typical for low-arc cathodic deposition. Even curve selection about half the total amount of indentations did not yield low standard deviations for hardness and Young's modulus. No single curve for AlCrSiN was even appropriate for analysis. Another deposition technique obeying better surface properties is therefore advisable.

The measurements for CrAlTiN at 150nm did not follow the expected trend. One would expect a higher hardness and Young's modulus, lying in between the values for 100nm and 200nm. Measuring the data again is recommended, although the data is not used for simulations.

In this report plastic material properties of the coatings are investigated with a finite element model. To this purposes a linear work hardening model is assumed. For each coating approximately 40 simulations of 30 minutes each are performed for different sets of plastic material properties (yield strength and tangent modulus). The maximum load and residual depth of the simulations is compared with the maximum load and residual depth of the experiments for each simulation and the best match is chosen to be the solution. It might be possible to perform optimization studies in ANSYS Workbench instead of changing input parameters (the plastic material properties) by hand each simulation. This is something that could be investigated in future studies, especially when material properties at different temperatures are to be determined.

Using measurement data of CrAlTiN at a depth of 250nm to determine the plastic material properties is also recommended. In this analysis only data at a depth of 200nm is taken into account, but 250 nm depth is also close to the 10% thickness of the coating (which is 2.4 µm). For CrAlN and CrAlSiN only data at 200nm depth was available.

Investigation of non-linear hardening might be useful as well. For this study it was not taken into account as computational resources were limited. It was tried to use multi-linear hardening though, but simulation time was an issue.

A SEM analysis of the tip rounding is preferred. Tip rounding has a big influence on load-displacement curves and thus on the plastic material properties found by simulation. It is for that reason that the plastic material properties determined in this report are not certain.

References

1. *Structure and tribological properties of AlCrTiN coatings at elevated temperature.* **Polcar, T. and Cavaleiro, A.** 2011, Surface & Coatings Technology 205, pp. 107-110.

2. *High temperature tribological properties of CrAlN, CrAlSiN and AlCrSiN coatings.* **Polcar, T. and Cavaleiro, A.** 2011, Surface & Coatings Technology 206, pp. 1244-1251.

3. *High temperature properties of CrAlN, CrAlSiN and AlCrSiN coatings - Structure and oxidation.* **Polcar, T. and Cavaleiro, A.** 2011, Materials Chemistry and Physics 129, pp. 195-201.

4. *An improved technique for determining hardness and elastic modulus using load and displacement sensing indentation experiments.* **Oliver, W.C. and Pharr, G.M.** 1992, Journal of Materials Research 7, pp. 1564-1583.

5. *Mechanical testing of thin films.* **Brotzen, F.R.** 1994, International Materials Reviews 39, pp. 24-45.

6. **Materials, Micro.** *NanoTest User Manual.* [Manual] s.l. : Micro Materials, 2013.

7. *Simulation of Berkovich nanoindentation experiments on thin films using finite element method.* **Lichinchi, M., et al., et al.** 1998, Thin Solid Films 312, pp. 240-248.

8. **ANSYS, Inc.** *ANSYS Mechanical User Guide Release 14.5.* [Manual] Canonburg : ANSYS, Inc, 2012.

9. **Sezer, Serhan.** *An Evaluation of ANSYS Contact Elements.* Istanbul : s.n., 2002.

10. **Johnson, D.H.** *Principles of Simulating Contact Between Parts using ANSYS.* [Document] Erie : ANSYS, Inc.

11. *Effect of Friction in Indentation Hardness Testing: a Finite Element Study.* **Cai, X.** 1993, Journal of Materials Science Letters 12, pp. 301-302.

12. **Tabor, D.** Indentation Hardness and Its Measurement: Some Cautionary Comments. [book auth.] Blau PJ and Lawn BR. *Microindentation Techniques in Materials Science and Engineering.* 1985.

13. **Fischer-Cripps, Anthony C.** *Introduction to Contact Mechanics.* New York : Springer Science+Business Media, LLC, 2007. ISBN10 0-387-68187-6 / ISBN13 978-0-387-68187-0.

Appendices

Width

In figure X it is clearly visible that doubling the width of the coating body in the finite element model has only a small influence on the load-displacement curve. The curve is stretched just a little bit to a higher load.

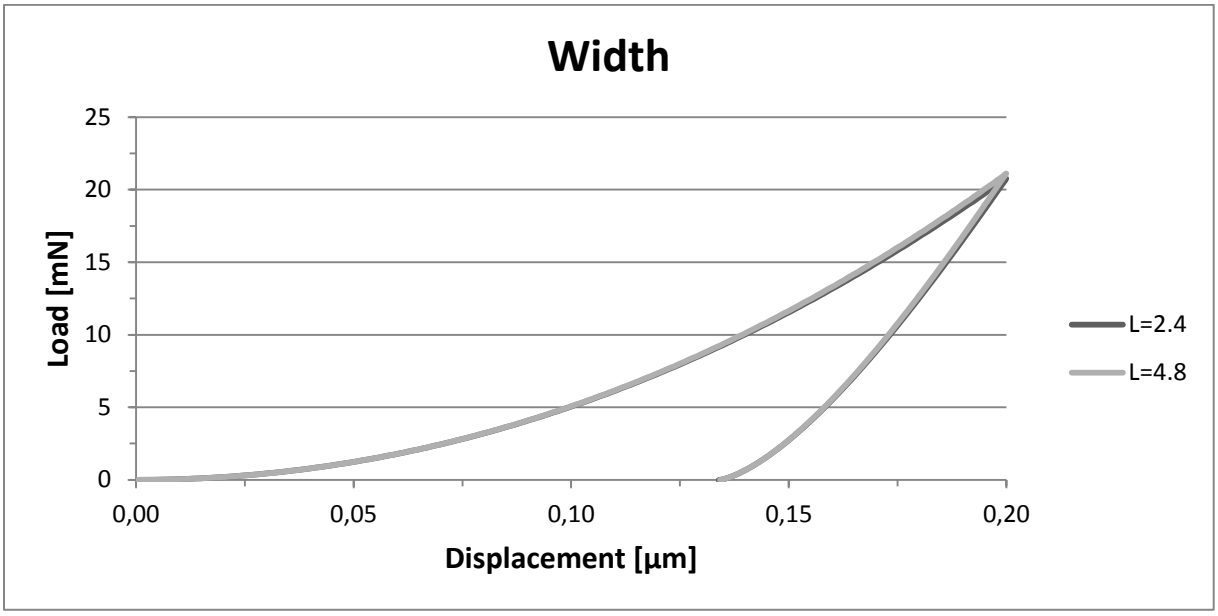

Figure 21 - Influence coating width on load-displacement curves

Boundary Conditions

In figure X it is clearly visible that the boundary condition in x-direction on the edge of the coating body in the finite element model has only a small influence on the load-displacement curve. The curve is stretched just a little bit to a lower load.

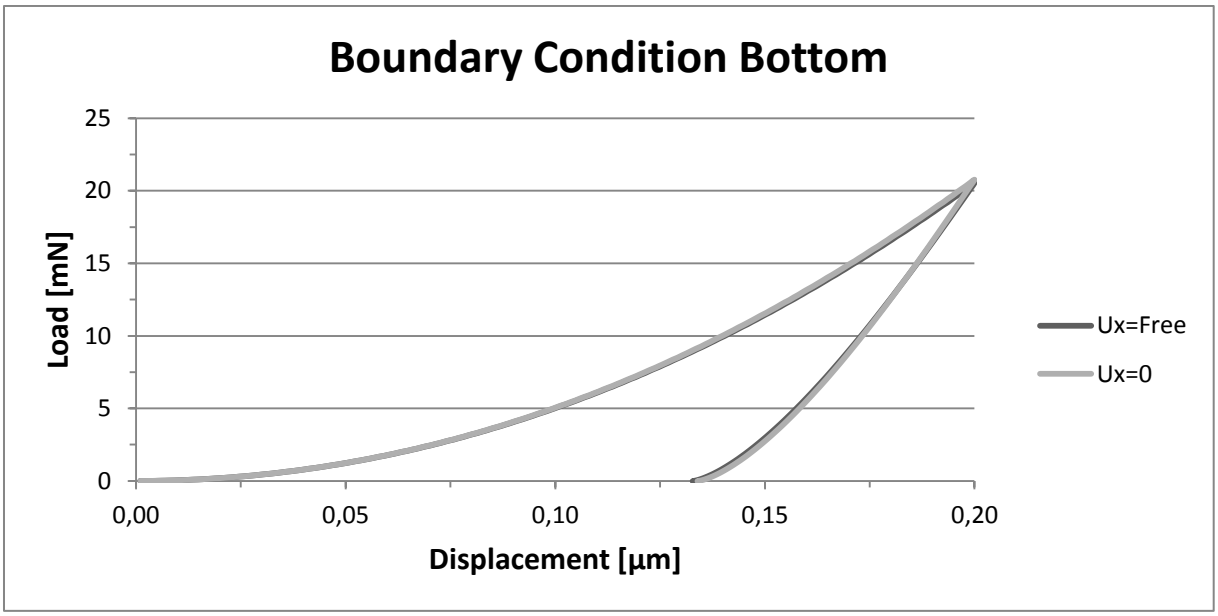

Figure 22 - Influence boundary condition boundary edge on load-displacement curves